ELSEVIER

Polymer 42 (2001) 2531–2542

polymer

www.elsevier.nl/locate/polymer

Gas sorption and transport in side-chain crystalline and molten poly(octadecyl acrylate)

Z. Mogri, D.R. Paul*

Department of Chemical Engineering and Texas Materials Institute, The University of Texas at Austin, Austin, TX 78712, USA

Received 30 June 2000; received in revised form 28 August 2000; accepted 28 August 2000

Abstract

The gas sorption and transport properties of poly(octadecyl acrylate) are described for the semi-crystalline and molten states. The change in permeability upon traversing the melting point, or permeation switch, was observed to be as high as two orders of magnitude depending on the penetrant. Analysis of gas transport is explained using the Michaels and Bixler model for semi-crystalline polyethylene. This analysis shows chain immobilization of the amorphous phase by surrounding crystals to play a significant role in describing the penetrant-dependent permeation switch in this side-chain crystalline polymer. Traditional two-phase models describing crystallites as impenetrable barriers with no effect on amorphous phase properties may explain solubility in this system but do not describe diffusion. The dependence of transport parameters on polymer composition, e.g. side-chain length, is also discussed.

Keywords: Side-chain crystalline polymers; Octadecyl acrylate; Permeation switch

1. Introduction

The sorption and diffusion of penetrant molecules (e.g. gases, vapors or liquids) in semi-crystalline polymers has been a subject of interest for several decades. Much of the understanding of how crystallinity affects these properties stem from experimental studies of polymers where it is the chain backbone itself that crystallizes, i.e. main-chain crystalline polymers, such as polyethylene (PE) and others [1–12]. By comparison, very few studies have focused on polymers with side-chain crystallinity [13–15].

In both cases, crystallite size and shape, overall crystalline morphology, and the degree of crystallinity, all of which are influenced by the thermal history of the polymer, are expected to have an important influence on permeation processes. These factors have been accounted for using classical two-phase models [16,17]. The most widely used description continues to be the one proposed by Michaels and Bixler 40 years ago [18]. The basic concept is that the crystallites represent a non-sorbing, non-permeable phase; hence, all diffusion occurs in the amorphous phase. However, only a limited number of studies have been done above the melting point or using an amorphous analog of the semi-crystalline polymer so that the properties of the amorphous phase are well known [1,3,4,12,18–21]. Furthermore, there is evidence that the presence of the crystallites affects the nature of the amorphous phase.

Side-chain crystalline polymers and in particular long side-chain poly(*n*-alkyl acrylate)s and poly(*n*-alkyl methacrylate)s are well documented in the literature [14,22–26]. Extensive studies of their physical, thermal and structural properties have been reported, but a complete understanding of the packing of the side-chains [27,28] and how the backbone organization [29–32] and mobility are affected by the crystallites have not yet evolved. Because of these and other factors there may be significant differences in how side-chain versus main-chain crystallinity affect penetrant sorption and diffusion.

This paper reports an in-depth study of gas sorption and transport behavior of poly(octadecyl acrylate) or PA-18. Side-chain crystalline polymers of this type show dramatic changes in many properties upon traversing the melting point. The resulting switch effect makes these materials of interest for biomedical, agricultural and packaging applications [33–38]. The objective here is to examine the thermal switch properties of PA-18. Ultimately, the aim of this research is to understand how to design polymers, e.g. side-chain length, backbone stiffness, etc. to obtain specific switch properties such as the magnitude and breadth of the

* Corresponding author. Tel.: +1-512-471-5392; fax: +1-512-471-0542.
E-mail address: drp@che.utexas.edu (D.R. Paul).

0032-3861/01/$ - see front matter
PII: S0032-3861(00)00657-1

permeation jump. These ideas will be elucidated with the Michaels and Bixler model recalling the structural considerations of the side-chain packing.

2. Background

2.1. Structure and properties of poly(n-alkyl (meth)acrylate)s

Early work on the thermal properties of polymer series with varying side-chain lengths established a critical number of methylene groups to develop crystallinity [22] which for the poly(*n*-alkyl acrylate)s is approximately 9–10. Beyond this, the melting point (T_m) and degree of crystallinity (x_c) for a given polymer backbone, increase as the side-chain length increases. It appears that the 9–10 methylene units closest to the backbone reside in an amorphous state while the methylene groups beyond this limit are accommodated in the crystalline lattice; thus, the crystallites become thicker (increases T_m) and occupy a larger fraction of the material (increases x_c). Some aspects of these materials are greatly affected by the nature of the chain backbone, e.g. stiffness. Poly(alkyl methacrylate)s series show lower T_m and x_c than poly(alkyl acrylate)s of the same side-chain length [22,27]. Copolymerization can be used to alter backbone stiffness, e.g. butadiene-*co*-alkyl acrylate has a more flexible backbone than styrene-*co*-alkyl acrylate [39,40]; it is generally accepted that a stiff backbone reduces conformational freedom of the side-chain which allows fewer methylene groups to crystallize [23,39,40].

The structure of side-chain crystalline polymers has been studied by both wide-angle X-ray diffraction and small-angle X-ray scattering. It is generally argued the side-chains of poly(alkyl (meth)acrylate)s pack in a hexagonal crystal structure. Platé has proposed that the polyacrylates exhibit a two-layer structure, whereas the polymethacrylates display a one-layer structure [27,41,42]. These researchers have argued that the main-chain flexibility determines the layer structure. The added bulkiness of the methyl groups tends to disrupt the packing leading to the one-layer arrangement. It has been claimed for both series that the side-chains pack end to end and that the backbone participates in crystallization in the acrylate polymers [27,28]. Others contend that the backbone does not take part in crystallization and that the side-chains intercalate [28]. Furthermore, investigations of crystal structure for both flexible (e.g. polyesters) and rigid (e.g. poly(phenylene terephthalate)s) comb-like polymers have shown the side-chains to intercalate while the backbone may or may not take part in the crystallization [43,44]. Future small-angle X-ray studies are planned to gain more insights about this issue.

2.2. Gas sorption and transport in semi-crystalline rubbery polymers

Gas permeation through dense polymers occurs by a solution-diffusion mechanism. The penetrant sorbs into the polymer at the upstream surface, diffuses through the membrane and desorbs from the opposite surface. The permeability coefficient is the product of solubility and diffusion coefficients

$$P = DS \tag{1}$$

The diffusion coefficient is a kinetic factor that reflects the mobility of the penetrant in the polymer phase while the solubility coefficient is thermodynamic in nature and is a function of polymer-penetrant interactions and the condensibility of the gas. The temperature dependence of these coefficients are usually described by

$$D = D_0 \exp\left(\frac{-E_d}{RT}\right) \tag{2}$$

$$S = S_0 \exp\left(\frac{-\Delta H_s}{RT}\right) \tag{3}$$

$$P = P_0 \exp\left(\frac{-E_p}{RT}\right) \tag{4}$$

where $E_p = E_d + \Delta H_s$ is the overall activation energy for permeation, E_d is the activation energy for diffusion and ΔH_s is the heat of sorption.

These parameters depend on the structure and morphology of the polymer matrix. PA-18 is semi-crystalline at temperatures below its melting point of 50°C and has a glass transition temperature well below the range of temperatures of interest here. Thus, this polymer may be thought of in terms of two distinct phases (i.e. crystalline and rubbery) below the melting point.

Sorption of gases in polymers that are above their glass transition temperature are well described by Henry's law

$$C = Sp \tag{5}$$

where S is the Henry's law constant, C is the equilibrium concentration of the penetrant in the polymer and p is the pressure of the penetrant in the gas phase. It has been proposed that gas solubility in semi-crystalline PEs with varying degrees of crystallinity is well described by the following equation

$$S = S^* \alpha \tag{6}$$

where α is the volume fraction of the amorphous polymer phase [18,45,46]. These results imply that S^* is the solubility coefficient for completely amorphous PE and that the solubility coefficient is exactly zero in the PE crystal. This model was validated by the work of McCrum who measured the solubility of large penetrants in semi-crystalline and molten PE. The value of α based on these measurements agreed well with independent measurements of α based on density [3]. However, calculated values of α based on solubility measurements of N_2 and CO_2 in polybutadiene did not agree with the density value of α [1]. Puleo and Paul showed that there is an appreciable amount of gas sorbed

by the crystals of poly(4-methyl-1-pentene) [47]. These results can be understood in terms of the much more open structure of the crystals whose density is essentially the same as that of the amorphous phase compared to PE whose crystals are 17% more dense than the amorphous phase. Additionally, penetrants have been shown to sorb in the crystals of the δ form of syndiotactic polystyrene [48,49].

It is generally assumed that Eq. (6) applies for most semi-crystalline polymers which implies that the presence of the crystals does not affect the amorphous phase, at least as far as gas solubility is concerned. Yet, Budzien et al. [19] predicted the solubility of gases in amorphous PE to be approximately a factor of 2 greater than that predicted by the Michaels and Bixler model [18]. These researchers noted that crystallite constraining effects on the amorphous phase might play a large part in gas solubility in addition to gas diffusivity. The crystals do seem to have two separate effects on the diffusion coefficient as shown in the work of Michaels and Bixler on PE [18]. The crystallites act as impenetrable barriers to the penetrant which can be accounted for by a tortuosity or geometric impedance factor, τ; i.e. the penetrant must follow an elongated path due to the crystallites in order to diffuse through the polymer. In addition, the crystallites seem to impair the mobility within the amorphous phase and leads to a higher activation energy for diffusion through the amorphous phase; Michaels et al. introduced a chain immobilization factor β to account for this effect. According to this model, where D^* is the diffusion coefficient in the amorphous phase without any perturbation due to the crystallites, the overall diffusion coefficient in a semi-crystalline polymer is given by

$$D = D^*/\tau\beta \tag{7}$$

Limited studies suggest that τ is a function of α while β and D^* depend on the molecular diameter of the penetrating gas molecule. The tortuosity must also be dependent on crystallite size and shape, the size distribution and how the crystallites are organized in space. The tortuosity has not been correlated to any of these properties in prior work but the significance of these supramolecular parameters must not be overlooked. In principle, the effect of these details of crystal structure on the tortuosity part of the model can be accounted for quite rigorously using theories for two-phase composites [16,17,50]. However, this type of modeling does not shed any light on the so-called "chain immobilization" effect, i.e. β.

According to the above model, the permeability of the purely amorphous phase, P^*, is given by

$$P^* = D^*S^* \tag{8}$$

One of the real limitations to our current understanding of permeation in semi-crystalline polymers is that rarely has P^*, D^* or S^* been measured directly. One experimental approach would be to measure these quantities above T_m and extrapolate to temperatures of interest below T_m. This method is used here for PA-18, but it is usually not practiced for polymers with very high melting points. In their work, Michaels et al. assumed that amorphous PE has similar diffusion properties as natural rubber. The validity of this assumption is certainly open to debate. Other approaches are needed to refine the model.

3. Materials and methods

Octadecyl acrylate monomer was generously donated by Landec Corporation and was polymerized, as received, in heptane (Fisher Scientific) at 60°C for 24 h. The monomer and initiator concentrations were approximately 35 and 0.35 wt.%, respectively. The polymer was precipitated into cold methanol (EM Science) and then purified by reprecipitation in the heptane/methanol system three times.

Poly(2,6-dimethyl-1,4-phenylene oxide) (PPO) was generously provided by General Electric Plastics (intrinsic viscosity = 0.46 dl/g; $M_w = 46{,}000$). Anopore™ (Whatman) porous ceramic membrane discs (pore diameter is 0.02 μm) were used without the annular polypropylene support ring.

Films were solution cast on glass plates from a toluene solution containing 10 wt.% PA-18 in a fume hood. The resulting highly brittle films of semi-crystalline polymer were allowed to dry for approximately 2 days. They were then placed in a vacuum oven at room temperature for 24 h before use. PPO was coated on the Anopore™ discs by a modified casting knife technique. Approximately 2 ml of a 15 wt.% solution of PPO in trichloroethylene (Fisher Scientific) was deposited evenly and quickly onto an Anopore™ disc. Excess solution was scraped off using a Scoopula® (Fisher Scientific) leaving a thin film on the disc. The composite was allowed to dry in the fume hood and was then placed in a vacuum oven at 100°C for 24 h to remove residual solvent. These composites were subsequently stored in air at about 65°C for 3–10 days before use.

Cast films of PA-18 were placed on a PPO-coated Anopore porous support and melted in the permeation cell to form a three-layer composite membrane. The resistance in the porous layer was negligible while the thin PPO coating was measured for its resistance prior to and after measurements of the entire composite membrane. Through a series resistance model, the permeability of PA-18 was calculated. Permeation and sorption measurements were made in the molten state and then the composite was removed from the cell and placed on a hot stage. The membrane was melted again and cooled at a certain rate for a reproducible thermal history. Measurements were made for the solid polymer, and then eventually again in the molten state. The concerns and issues leading to the choice of this assembly and the measurement techniques are discussed in detail in a previous publication [51].

Permeability measurements were carried out as a function of temperature in pressure-rise constant volume systems.

Table 1
Effect of thermal history on the thermal and physical properties of PA-18

Thermal history	T_m (°C)	ΔH_f (cal/g)	x_c [a]	Notes
As cast	55	25.1	0.48	This work
0.1°C/min [b]	52	21.6	0.41	This work
1.0°C/min [b]	50	19.3	0.37	This work
– [c]	56	21.3	0.41	Ref. [22]
– [c]	53	23.4	0.45	Ref. [27]

[a] The degree of crystallinity is calculated from Eq. (11).
[b] Rate of cooling from the melt.
[c] History not described.

These systems have been previously described in detail elsewhere [52]. The gases used, He, H_2, O_2, N_2, CH_4 and CO_2, were obtained from Praxair and Air Liquide with at least 99.9% purity. All measurements were made at 2 atm upstream pressure. Solubility measurements were made via a pressure decay method as a function of temperature in a dual volume cell as described previously [52]. Measurements were made as a function of pressure up to at least 7 atm for both CH_4 and CO_2.

Melting points and heats of fusion of the side-chain crystalline polymers were determined using a Perkin–Elmer DSC-7 equipped with an intercooler for measurements starting from −40°C. All heating rates were 20°C/min while cooling rates were set at 0.1, 1.0 or 10°C/min to vary the thermal history of the sample. The thermal history of the actual membranes was varied by the use of two hot stages. One was a Mettler FP82HT hot stage with an FP80HT central processor equipped with an air line for cooling. Another was a Linkham TMS91 hot stage with a Linkham CS196 cooling system that utilized liquid N_2. Molecular weights of the synthesized polymers were obtained by gel permeation chromatography using polystyrene standards.

4. Results and discussion

4.1. Polymer characterization

The thermal properties of PA-18 having various thermal histories are shown in Table 1. The "as cast" polymer has the highest melting point and heat of fusion (ΔH_f). "As cast" films of PA-18 display preferred orientation of the crystallites which may lead to these high values [51]. As the cooling rate from the melt is increased, the melting point and heat of fusion decrease. This translates to a lower degree of crystallinity, x_c, for the higher cooling rate. This degree of crystallinity was calculated from the following

$$x_c = \frac{(\Delta H_f)}{(\Delta H_{f0})} \tag{11}$$

where ΔH_f was measured by DSC (expressed in units of cal/g of sample) and the value of ΔH_{f0} is 52.5 cal/g of crystal [22,53]. This value was taken from studies of the melting behavior of long chain *n*-alkanes that exhibit a hexagonal crystal structure. It is well accepted that long side-chain polyacrylates crystallize into such a lattice. Moreover, X-ray powder diffraction of PA-18 reveals an absence of peaks known to indicate an orthorhombic or triclinic modification [54,55]. Also, an FT-IR scan of PA-18 shows a peak characteristic of the hexagonal lattice [55]. The thermal properties for this polymer agree well with previous published reports [22,27].

4.2. Gas permeation

Representative graphs of the permeation switch behavior of PA-18 are shown in Fig. 1. The data below T_m were obtained using a film cooled from the melt at 1°C/min in a hot stage. On heating, some pre-melting of the crystals occurs around 40°C, but a rather sharp transition is observed in the range of 45–50°C. It is important to note that the order of the measurements were made as mentioned in the previous section. The permeation properties of the semi-crystalline film depend somewhat on its thermal history; however, the permeation results in the molten state were the same before and after the solid state measurements.

A comparison of the various graphs in Fig. 1, reveals that the permeation jump depends on the nature of the gas; the effect of the penetrant on the magnitude of the permeation jump will be examined more closely in a subsequent section. At this point, it is useful to compare the magnitudes of the crystalline and molten state permeabilities to other structurally similar polymers. With the exception of the ester linkage, PA-18 is arguably similar to PE. The gas permeability of PEs of various levels of crystallinity have been reported

Table 2
Comparison of gas permeability coefficients for semi-crystalline PA-18 and various PEs. All values measured at 35°C and given in Barrers

Gas	PA-18 ($\alpha = 0.63$)	High-density PE ($\alpha = 0.23$)[a]	Medium-density PE ($\alpha = 0.57$)[a]	Low-density PE ($\alpha = 0.71$)[a]
He	8.24	1.68	7.77	25.0
H_2	8.35	–	–	–
O_2	1.18	0.64	5.06	19.4
N_2	0.29	0.24	1.85	7.36
CH_4	0.64	0.66	5.38	23.7
CO_2	4.25	2.52	21.0	77.8

[a] From Ref. [18].

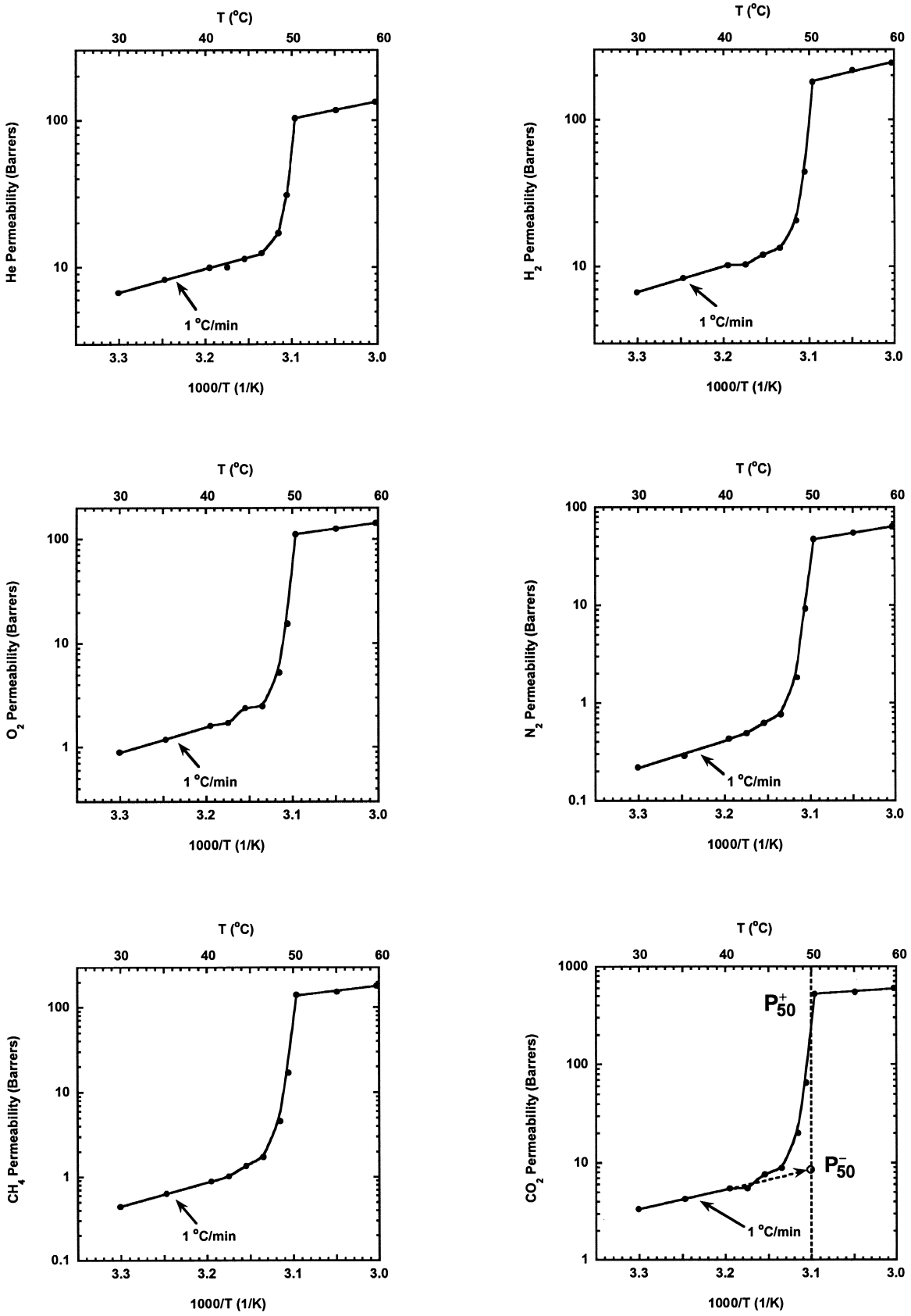

Fig. 1. He, H_2, O_2, N_2, CH_4 and CO_2 permeability (Barrers) of PA-18 as a function of temperature. The measurements were done in the order of: (1) molten state above 50°C; (2) cooling the molten polymer in a hot stage at 1°C/min; (3) semi-crystalline state from 30 to 40°C; and (4) intermediate state from 42 to 49°C. Extrapolations to 50°C in the molten and semi-crystalline states (P_{50}^{+} and P_{50}^{-}) form the basis for evaluating the permeation switch of this polymer.

Table 3
Comparison of activation energies for gas permeation for semi-crystalline PA-18 and various PEs

Gas	PA-18 ($\alpha = 0.63$)	High-density PE ($\alpha = 0.23$)[a]	Medium-density PE ($\alpha = 0.57$)[a]	Low-density PE ($\alpha = 0.71$)[a]
He	7.4 (kcal/mol)	7.1 (kcal/mol)	8.3 (kcal/mol)	8.4 (kcal/mol)
H_2	8.0			
O_2	11.2	8.4	10.2	9.8
N_2	12.6	9.5	11.8	11.2
H_4	13.1	9.7	11.3	10.9
CO_2	9.2	7.2	9.3	8.7

[a] From Ref. [18].

[18] and are compared to PA-18 in Table 2. PA-18 has a much lower permeability for all gases, with the possible exception of helium, than PE materials of comparable crystallinity. Of course, there are significant physical differences between PE and this poly(*n*-alkyl acrylate), in addition to the chemical structural differences, that deserve note. First, PE crystallizes in an orthorhombic lattice while PA-18 adopts a hexagonal crystal structure. Second, it is the side-chains in PA-18 that crystallize while for PE it is the main-chain. The crystalline state morphologies of the two materials are no doubt quite different. Note that activation energies for permeation in PA-18 are generally slightly higher than for the PEs for various crystallinities as seen in Table 3.

A comparison of just the effect of the polymer repeat unit structure on gas permeability properties is best done in the amorphous state where the effects of crystallinity are absent. The amorphous state gas permeability coefficients of poly(methyl acrylate) (PMA), natural rubber and PA-18 are compared at a common temperature of 35°C in Table 4. Note that for all gases considered, PA-18 is substantially more permeable than PMA. The effect of side-chain length on the gas permeability properties of poly(*n*-alkyl acrylate)s will be described more completely in a future paper. Amorphous PA-18 is also 1.5–2 times more permeable than natural rubber. As seen in Table 5 the activation energies for permeation in amorphous PA-18 are lower than for natural rubber.

There are several ways to quantify the magnitude of the permeation switch effect shown in Fig. 1. The method chosen here compares the permeability coefficient for a given penetrant in the molten state to that in solid state at a specified temperature. The choice of temperature is arbitrary but significantly affects the ratio of these permeability coefficients as discussed later. In the present case, a convenient temperature is the melting point of the polymer, 50°C for PA-18. The molten state permeation data are extrapolated to 50°C and the resulting value designated as P_{50}^{+}, where the " + " represents the amorphous or molten state. A similar extrapolation was done for the semi-crystalline state with the value at 50°C designated P_{50}^{-} where the " − " represents the semi-crystalline or solid state data. This procedure is shown graphically in Fig. 1. The ratio of these two parameters, P_{50}^{+}/P_{50}^{-}, is then used as the measure of the magnitude of the permeation jump. It is seen in Fig. 2 that this ratio correlates quite well with the Lennard-Jones collision diameters of the penetrant gas molecules studied. The ratio changes by about an order of magnitude going from He to CH_4.

The collision diameter is the effective diameter of the gas molecule as it freely rotates in the gas phase. For non-spherical molecules it is useful to use the "kinetic diameter" which more nearly measures its smaller dimension. For the gases in Fig. 2, the kinetic diameters are essentially the same as the Lennard-Jones collision diameters except for the more cylindrical CO_2 molecule whose kinetic diameter is 3.3 Å. The open circle in Fig. 2 represents the permeability jump for CO_2 replotted at its kinetic diameter. Use of either value does not change the essential trend of the

Table 4
Comparison of gas permeability coefficients for PA-18, PMA and natural rubber in the amorphous state. All values measured at or extrapolated to 35°C and expressed in Barrers

Gas	PA-18	PMA[a]	Natural rubber[b]
He	68.8	10.6	43.3
H_2	113		71.1
O_2	75.0		36.2
N_2	29.1	0.187	13.1
CH_4	90.8	0.235	45.0
CO_2	428	7.20	183

[a] From Ref. [57].
[b] From Ref. [58].

Table 5
Comparison of activation energies for gas permeation for molten PA-18 and natural rubber

Gas	PA-18	Natural rubber[a]
He	5.4 (kcal/mol)	6.1 (kcal/mol)
H_2	6.3	6.8
O_2	5.2	7.5
N_2	6.3	8.8
CH_4	5.6	7.4
CO_2	2.7	6.1

[a] From Ref. [58].

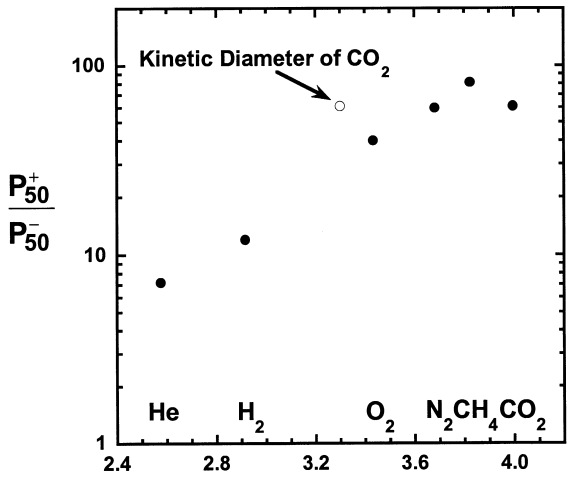

Fig. 2. Magnitude of the permeation switch for PA-18, P_{50}^{+}/P_{50}^{-} as a function of the Lennard-Jones collision gas diameter. The open point is the value for CO_2 plotted at its kinetic diameter.

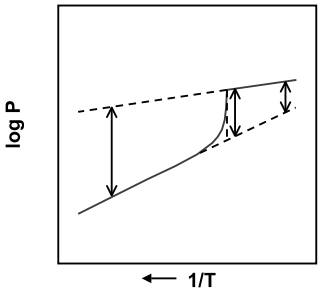

Fig. 3. A typical Arrhenius plot of permeability versus temperature for a polymer in the semi-crystalline and molten states. The dashed lines represent extrapolations of the semi-crystalline and molten state data (solid lines). This illustrates the importance of the temperature choice when calculating the permeation switch.

data, but it seems that a dimension intermediate between the collision diameter of 4.0 Å and the kinetic diameter of 3.3 Å would better represent CO_2 in this plot.

It is important to emphasize that the temperature, T, selected to form the ratio, P_T^{+}/P_T^{-}, will affect the value of the ratio since the permeation activation energies in the melt and semi-crystalline state are different as illustrated schematically in Fig. 3. The dashed lines represent extrapolations of the data above and below T_m. The logarithmic distance between these lines, i.e. $\log(P_T^{+}/P_T^{-})$, clearly depends on the choice of T. The melting point of the polymer seems to be a reasonable choice of temperature for forming this ratio.

The simple two-phase model for gas permeation through semi-crystalline polymers, based on the concepts of the theory of composites, envisions the crystallites as impenetrable barriers to permeation, with no constraining effect on the amorphous phase. In this view, the crystallites reduce the volume available for diffusion and create a tortuous path for the penetrant. The large effect of the penetrant on the permeation jump shown in Fig. 2 cannot be explained by such a simple model. If the crystallites act only as physical obstacles, then upon melting, the permeability of the penetrant should increase, irrespective of its nature or size, due to the increase in the volume or reduction in tortuosity for diffusion. However, Michaels and Bixler in their work on PE found departure from the simple model, i.e. the permeability reduction due to crystallinity was found to be dependent on the size of the penetrant as seen here.

To compare the permeation switch values of PA-18 to PE, an amorphous analog representative of the molten properties of PE is needed since these properties are not available for the gases of interest here. There are a variety of amorphous polymers with structural similarity to PE; Michaels and Bixler selected natural rubber for this purpose. A more direct assessment of the gas permeation properties of amorphous PE is needed, but for now we use data for natural rubber for this analysis, as suggested by Michaels and Bixler.

As seen in Table 6 the estimated permeation switch for PE depends strongly on its degree of crystallinity or amorphous volume fraction α. The magnitude of the permeability ratios for the larger penetrants in high density PE ($\alpha = 0.23$) is very similar to that of PA-18. However, the high-density PE has three times the level of crystallinity as PA-18. The PA-18 shows much higher permeation jump values than the medium density PE. Even the latter is still more crystalline. Based on this limited comparison, it appears that side-chain crystallinity may lead to larger reductions in permeability than main-chain crystallinity, compared at the same level of crystallinity. Furthermore, the effect of penetrant size on the value of P_{50}^{+}/P_{50}^{-} is much larger for PA-18 than any of these PEs, at least

Table 6
Comparison of values of P_{50}^{+}/P_{50}^{-} for PA-18 with various PEs; for the latter, the P_{50}^{-} values are from the work of Michaels and Bixler [18] while the P_{50}^{+} values are approximated by data for natural rubber [58]

Gas	PA-18 ($\alpha = 0.63$)	High-density PE ($\alpha = 0.23$)	Medium-density PE ($\alpha = 0.57$)	Low-density PE ($\alpha = 0.71$)
He	7.19	23.9	4.72	1.45
H_2	12.0	–	–	–
O_2	40.0	52.7	5.83	1.57
N_2	59.6	52.8	5.64	1.49
CH_4	81.5	57.0	6.22	1.46
CO_2	61.1	66.8	6.85	1.93

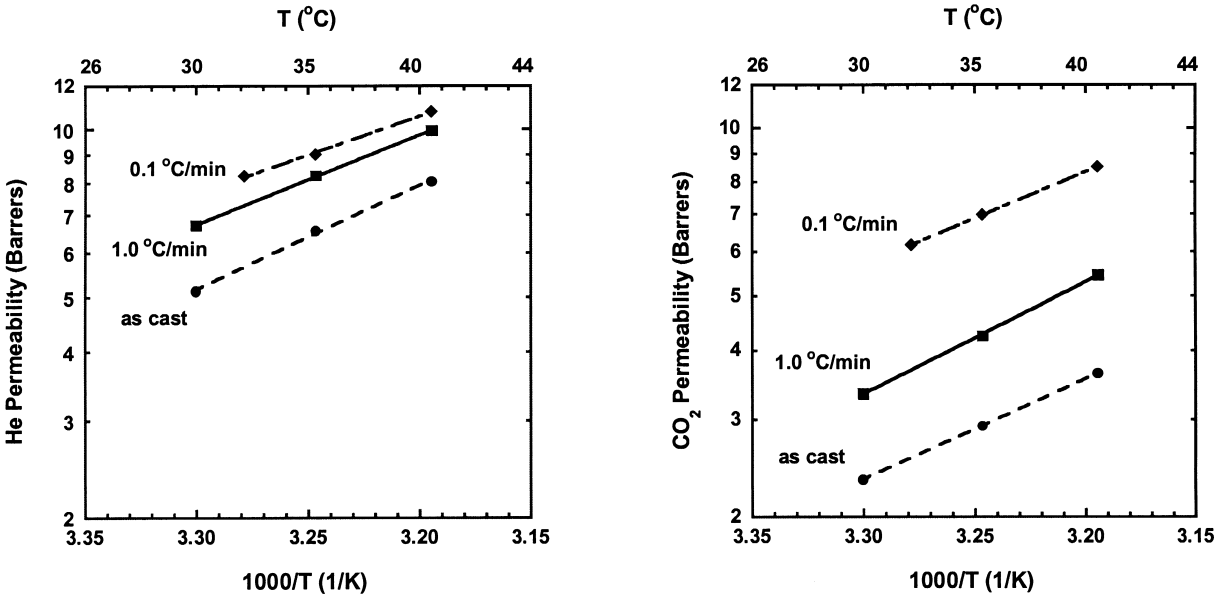

Fig. 4. He and CO_2 permeability as a function of temperature in the semi-crystalline state for different thermal histories. Upon comparison with Table 1, the trend in the semi-crystalline state permeability does not follow the expected dependence on the level of crystallinity.

based on the natural rubber approximation. The source of the penetrant dependence can be rationalized in terms of the modified model proposed by Michaels and Bixler. The ratio P_{50}^{+}/P_{50}^{-} is equivalent to P^{*}/P at 50°C in terms of the notations used in Eqs. (1) and (8). Combining these with Eqs. (6) and (7) leads to

$$\frac{P_{50}^{+}}{P_{50}^{-}} = \frac{P^{*}}{P} = \frac{\tau\beta}{\alpha} \tag{12}$$

Recall that the tortuosity, τ, is a simple geometric parameter describing how crystallite size, shape and orientation reduces the rate of penetrant diffusion which in principle, can be predicted by an appropriate two-phase composite theory. The amorphous volume fraction, α, can be independently measured by calorimetric techniques, volumetric techniques, etc. The chain immobilization factor, β, was introduced to account for the possibility that the presence of the crystallites change the properties of the amorphous phase, e.g. chain segmental motions, and has been shown to depend on the size of the gas molecule [18]. By measuring the gas solubility for the polymer in the semi-crystalline and molten states, one can test the validity of Eq. (6). From appropriate solubility and permeation data, the diffusion coefficients can be calculated in each of these states to obtain the product $\tau\beta$. This product cannot be separated experimentally without some assumptions; however, if the crystallite structure were known in sufficient detail and corresponding composite theory were available, then τ could be calculated permitting the absolute value of β to be obtained.

Before attempting to isolate any of these effects, it is instructive to examine the effect of thermal history on the permeability properties and the permeation switch behavior for PA-18. Samples with three different histories are compared: an "as cast" film and two others that were melted and cooled at different rates, i.e. 1 and 0.1°C/min. Fig. 4 shows the permeability of He and CO_2 are affected by this history. When combined with the physical characteristics in Table 1, an unusual trend is revealed. The "as cast" film which has the highest degree of crystallinity shows the lowest permeability, as might be expected. However, the film cooled from the melt at 0.1°C/min has a higher crystallinity *and* a higher permeability compared to the film cooled at 1°C/min. Because the molten state permeability is independent of this history, the magnitude of the permeation switch effect, i.e. P_{50}^{+}/P_{50}^{-}, shown in Fig. 5 reflects the trends seen in Fig. 4. Thermal history seems to affect the behavior of larger molecules more than the smaller ones. In fact, when comparing the extremes ("as cast" to 0.1°C/min), there is at least a two-fold difference in magnitude for these larger penetrants. This may reflect a lessening of chain immobilization effects, as these curves become less dependent on penetrant. These trends are a function of how fast the crystals are formed in these systems. This affects the particular size, shape and distribution of the crystals, which in part determines the overall morphology. To sort out these effects more fully requires better characterization of this morphology or texture and some probe of molecular mobility in the amorphous phase.

4.3. Gas sorption and diffusion

Fig. 6 shows typical sorption isotherms for CO_2 and CH_4 in PA-18 for the semi-crystalline, "as cast" ($T = 35$°C) and molten ($T = 50$°C) states. Since PA-18 is well above T_g at

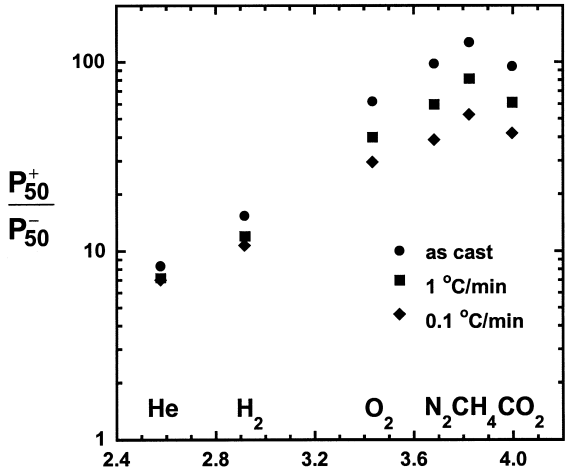

Fig. 5. Magnitude of the permeation switch for PA-18, P_{50}^{+}/P_{50}^{-}, plotted as a function of the Lennard-Jones collision gas diameter for different thermal histories. The shift in the magnitude of each curve stems from the semi-crystalline permeability, described in Fig. 4.

these temperatures, Henry's law describes the observed isotherms. The slopes of such plots are shown as a function of temperature for both the semi-crystalline and molten states in Fig. 7 and for "as cast" PA-18. The temperature dependence follows the form of Eq. (3); the heats of sorption calculated from the slopes of the solid lines drawn through the data are listed in Table 7. Similar experiments were also performed for other thermal histories, and the results are also shown in Table 7. Diffusion coefficients were calculated using Eq. (1) and are plotted as a function of temperature in Fig. 8. Again, the solid lines that reflect the Arrhenius temperature dependence and activation energies for diffusion are given in Table 7 for the thermal histories examined. In both Figs. 7 and 8, an extrapolation of the data to 50°C has been made from the semi-crystalline and molten states and the ratios for each gas are shown in Table 8. Comparing the "as cast" to the 1°C/min state in Table 7, the E_p and E_d for CH_4 and E_p for CO_2 increase, while the E_d for CO_2 decreases. One would expect lower activation energies for each gas from the "as cast" to the 1°C/min state based on the lower crystallinity of the latter state. The activation energy of permeation decreases when proceeding from the 1 to the 0.1°C/min states while the opposite should occur as the crystallinity increases. It is interesting to note that the trends in activation energy were also not clear for the variable crystallinity PE studied by Michaels and Bixler [18].

The ratio D_{50}^{+}/D_{50}^{-} can be equated to $\tau\beta$ according to Eq. (7). As seen in Table 8, the product of $\tau\beta$ is substantial for CH_4 and CO_2. This table also reveals a reduction in the $\tau\beta$ value for each gas compared to the "as cast" state. Coupled with Fig. 5 it seems that the chain immobilization plays a large role, but at a particular thermal history and for a sufficiently large molecule, this role may be diminished. However, it is experimentally difficult to separate the product of $\tau\beta$ into the particular values of interest. There is evidence from a variety of sources that the factor β makes a significant contribution to this product, see Tables 7 and 8. The activation energy for diffusion in the semi-crystalline state is almost twice that in the molten state. Independent evidence is provided by the dielectric relaxation measurements of Alig et al. for poly(octadecyl methacrylate) [56] which showed that relaxation of the dipole of the ester linkage (which always resides in the amorphous phase) was significantly retarded when the alkyl side-chains were in the crystalline state versus the molten state [56].

The solubility ratios in Table 8 are fairly constant for both CH_4 and CO_2 in the "as cast" state but drift apart in

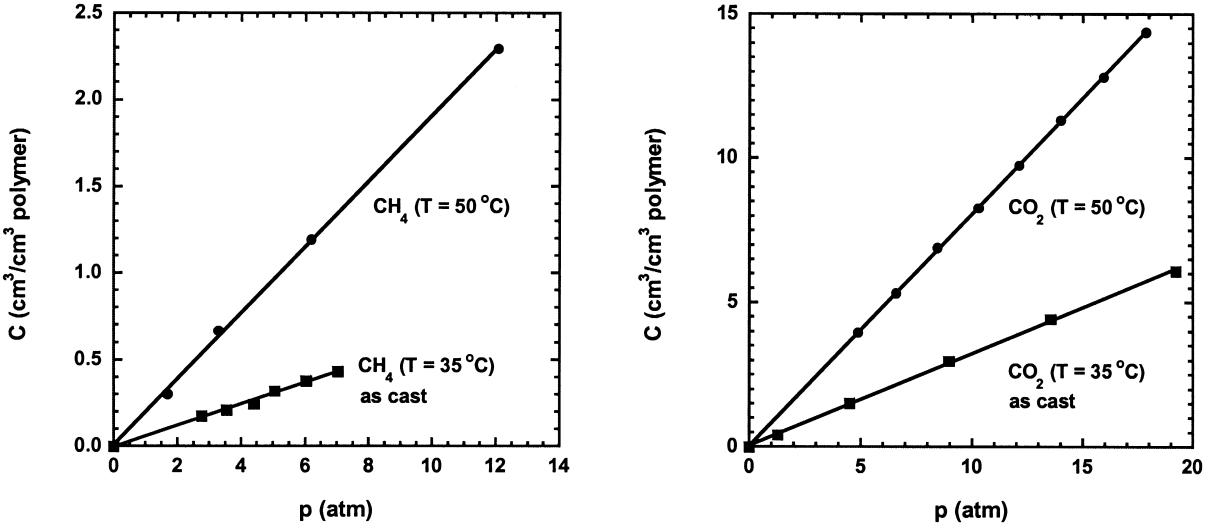

Fig. 6. Representative CH_4 and CO_2 sorption isotherms for PA-18 in both the semi-crystalline ("as cast") and molten states. The solubility follows Henry's law at the temperatures and pressures used.

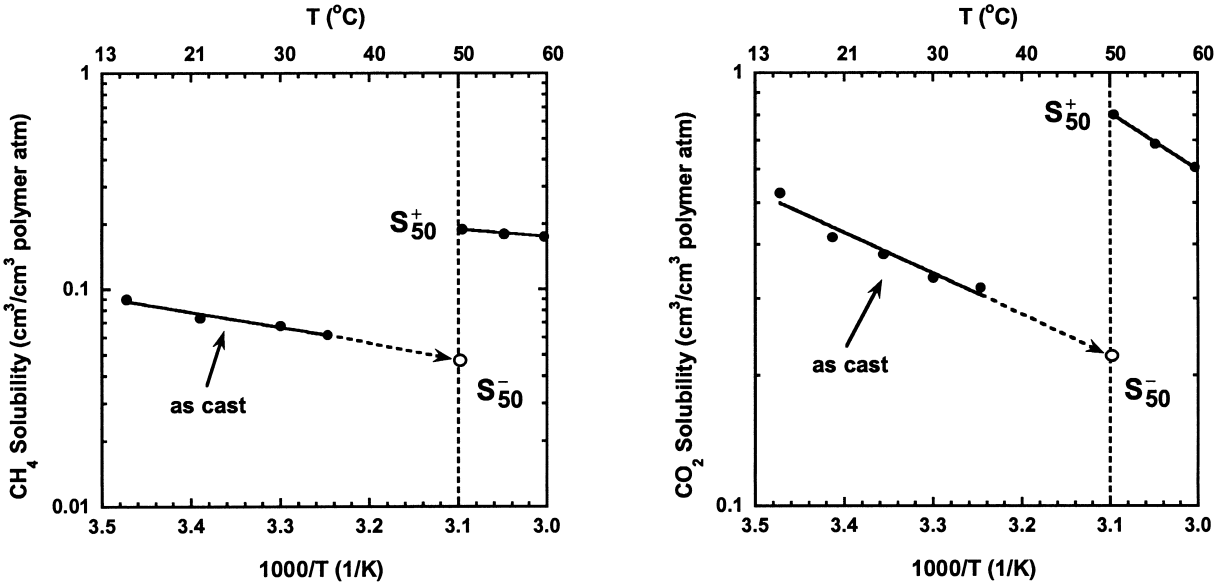

Fig. 7. CH_4 and CO_2 solubility coefficients for PA-18 as a function of temperature. The semi-crystalline state measurements were made with "as cast" films. Extrapolations to 50°C in the molten and semi-crystalline states (S_{50}^{+} and S_{50}^{-}) form the basis for evaluating the solubility switch of this polymer.

the 1°C/min state. Furthermore, these ratios are well below the α values calculated from DSC. According to the simple two-phase model given in Eq. (6), one expects the ratio of the solubility coefficient in the semi-crystalline relative to that in the amorphous state, i.e. S_{50}^{-}/S_{50}^{+}, to be equal to α as determined by thermal analysis. As seen in Table 8, these solubility ratios are of the order of one-half the value expected, with some minor variation depending on the thermal history and the gas. Strictly speaking, Eq. (6) was developed for polymers exhibiting main-chain crystallinity where the material in the crystal and amorphous phase is chemically identical. For side-chain crystalline polymers, this is not the case. The crystalline phase contains only hydrocarbon while the amorphous phase includes the ester linkage; thus there is a change in composition of the material the gas molecules "see" in the semi-crystalline versus the molten states. Below T_m there are 10 side-chain methylene groups plus the backbone in the amorphous state, while above T_m there are 18 methylene groups in the amorphous phase. Gas permeability data for these side-chain acrylates show a dependence on the side-chain length and arguably, gas solubility data must also show some dependence. These results will be reported in a subsequent publication.

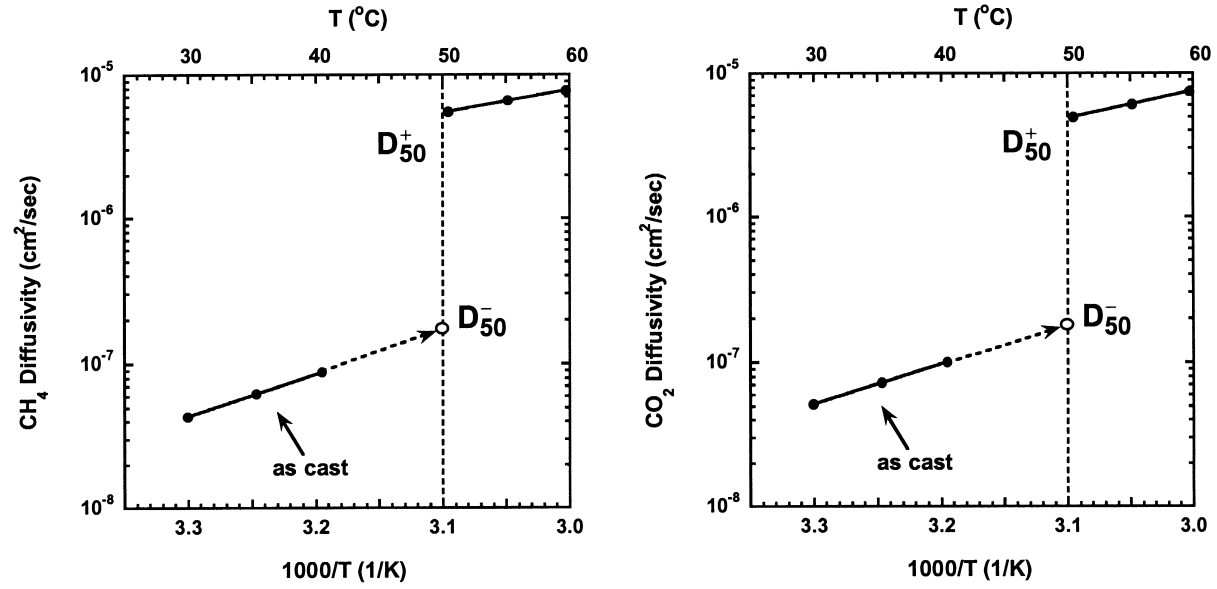

Fig. 8. CH_4 and CO_2 diffusion coefficients for PA-18 as a function of temperature calculated using the permeability and solubility data and Eq. (1). Extrapolations to 50°C in the molten and semi-crystalline states (D_{50}^{+} and D_{50}^{-}) form the basis for evaluating $\tau\beta$ for PA-18.

Table 7
Effect of thermal history on gas transport properties for different thermal histories of PA-18. Permeability values are measured at 35°C and expressed in Barrers

	CH_4				CO_2			
Thermal history	P	E_p	ΔH_s	E_d	P	E_p	ΔH_s	E_d
As cast	0.51	10.1 kcal/mol	−3.2 kcal/mol	13.3 kcal/mol	2.93	8.3 kcal/mol	−4.3 kcal/mol	12.6 kcal/mol
1°C/min	0.64	13.1	−2.6	15.7	4.25	9.2	−2.3	11.5
0.1°C/min	1.23	10.0	–	–	6.98	7.7	–	–
Molten state	90.8	5.6	−1.6	7.2	428	2.7	−6.0	8.7

Table 8
Comparison of thermal switch values for permeability, solubility and diffusivity of PA-18

		CH_4			CO_2		
Thermal history	α	P_{50}^{+}/P_{50}^{-}	S_{50}^{-}/S_{50}^{+}	$D_{50}^{+}/D_{50}^{-} = \tau\beta$	P_{50}^{+}/P_{50}^{-}	S_{50}^{-}/S_{50}^{+}	$D_{50}^{+}/D_{50}^{-} = \tau\beta$
As cast	0.52	128	0.26	32.6	95.1	0.28	26.3
1°C/min	0.63	81.5	0.31	25.2	61.1	0.37	22.5
0.1°C/min	0.59	52.5	–	–	41.9	–	–

It is interesting to note that to our knowledge, and based solely on experimental observations, only one study [3] has matched the values of α from both physical and solubility measurements. These researchers focused on PE in solid and molten form and used much larger penetrants than studied here. Cowling and Park, in their work with polybutadiene [1], noted lower solubility ratios for N_2 and CO_2 compared to α based on density measurements. These ratios were different based on the gas studied.

5. Conclusions

Side-chain crystallinity present in PA-18 gives rise to unique transport properties including a permeation switch at the melting point. The magnitude of the switch is penetrant dependent; chain immobilization of the amorphous phase is thought to be a major cause for this. This was demonstrated with lower activation energies for diffusion in the molten state compared to the semi-crystalline state and the dependence of $\tau\beta$ on the penetrant. The two-phase model may hold for sorption in these side-chain crystalline polymers, but does not hold for diffusion. The compositional change at the melting point of PA-18 is thought to affect the solubility switch value, possibly accounting for the discrepancy in α.

Acknowledgements

This research was funded by National Science Foundation grant number CTS 97-14305 administered by the Division of Chemical and Transport Systems — Separation and Purification Processes Program.

References

[1] Cowling R, Park GS. J Membr Sci 1979;5:199–207.
[2] Lasoski SW, Cobbs WH. J Polym Sci 1959;36:21–33.
[3] Lowell PN, McCrum NG. J Polym Sci, Part A-2 1971;9:1935–54.
[4] Lundberg JL, Wilk MR, Huyett MJ. J Polym Sci 1962;57:275–99.
[5] Michaels AS, Vieth WR, Barrie JA. J Appl Phys 1963;34:1–12.
[6] Michaels AS, Vieth WR, Barrie JA. J Appl Phys 1963;34:13–20.
[7] Mohr JM, Paul DR. Polymer 1991;32:1236–43.
[8] Naito Y, Mizoguchi K, Terada K, Kamiya Y. J Polym Sci, Part B: Polym Phys 1991;29:457–62.
[9] Van Amerongen GJ. J Polym Sci 1947;2:381–6.
[10] Vieth W, Wuerth WF. J Appl Polym Sci 1969;13:685–712.
[11] Barrer RM, Chio HT. J Polym Sci, Part C 1965;10:111–38.
[12] Durrill PL, Griskey RG. AIChE J 1996;15:106–10.
[13] Lee J, Kim H, Park J, Lee K. J Membr Sci 2000;167:67–77.
[14] Lee J, Park J, Lee K. J Polym Sci, Part B: Polym Phys 2000;38:823–30.
[15] Matsumoto A, Oki Y, Otsu Y. Polym J 1991;23:201–9.
[16] Cussler EL, Hughes SE, Ward WJ, Aris R. J Membr Sci 1988;38:161–74.
[17] Petropoulos JH. J Polym Sci: Polym Phys 1985;23:1309–24.
[18] Michaels AS, Bixler HJ. J Polym Sci 1961;50:413–39.
[19] Budzien JL, McCoy JD, Weinkauf DH, LaViolette RA, Peterson ES. Macromolecules 1998;31:3368–71.
[20] Paul DR, DiBenedetto AT. J Polym Sci, Part C 1965;10:17–44.
[21] Van Amerongen GJ. J Polym Sci 1950;5:307–32.
[22] Jordan EF, Feldeisen DW, Wrigley AN. J Polym Sci, Part A-1 1971;9:1835–52.
[23] Jordan EF, Artmyshyn B, Speca A, Wrigley AN. J Polym Sci, Part A-1 1971;9:3349–65.
[24] Jordan EF. J Polym Sci, Part A-1 1971;9:3367–78.
[25] Jordan EF, Riser GR, Artmyshyn B, Pensabene JW, Wrigley AN. J Polym Sci, Part A-2 1972;10:1657–79.
[26] Rehberg CE, Fisher CH. J Am Chem Soc 1944;66:1203–7.
[27] Platé NA, Shibaev VP. Comb-shaped polymers and liquid crystals. New York: Plenum Press, 1987.
[28] Hsieh HWS, Post B, Morawetz H. J Polym Sci: Polym Phys 1976;14:241–1255.
[29] Beiner M, Schröter K, Hempel E, Reissig S, Donth E. Macromolecules 1999;32:278–6282.

[30] Cowie JMG. Pure Appl Chem 1979;51:2331–43.
[31] Cowie JMG, Haq Z, McEwen IJ. J Polym Sci: Polym Lett 1979;17:771–7.
[32] Cowie JMG. Structure and transitions below and above T_g in polymers derived from itaconic acid derivatives. In: Keinath SE, Miller RL, Rieke JK, editors. International symposium on order in the amorphous state of polymers. Midland, MI: Plenum Press, 1987.
[33] Stewart RF, Greene LC, Bhaskar RK. US Patent No. 5,120,349, (1992) (Landec Labs, Inc.).
[34] Stewart RF. US Patent No. 5,129,180, (1992) (Landec Labs, Inc.).
[35] Stewart RF. US Patent No. 5,156,911, (1992) (Landec Labs, Inc.).
[36] Stewart RF, Mohr JM, Budd EA, Phan LX, Arul J. Temperature-compensating films for modified atmosphere packaging of fresh produce. In: El-Nokaly MA, Pratt DM, Charpentier BA, editors. Polymeric delivery systems: properties and applications, 520. Washington, DC: American Chemical Society, 1993.
[37] Stewart RF. US Patent No. 5,254,354, (1993) (Landec Corporation).
[38] Greene L, Phan LX, Mohr JM. Side-chain crystallizable polymers for temperature-activated controlled release. In: El-Nokaly MA, Piatt DM, Charpentier BA, editors. Polymeric delivery systems properties and applications, 520. Washington, DC: American Chemical Society, 1993.
[39] Hirabayashi T, Yokota K. Polym J 1987;19:1115–9.
[40] Hirabayashi T, Kikuta T, Kasabou K, Yokota K. Polym J 1988;20:693–8.
[41] Platé NA, Shibaev VP, Petrukhin BS, Zubov YA, Kargin VA. J Polym Sci, Part A-1 1971;9:2291–8.
[42] Platé NA, Shibaev VP. J Polym Sci: Macromol Rev 1974;8:117–253.
[43] Magagnini PL, Tassi EL, Andruzzi F, Paci M. Polym Sci 1994;36:1502–15.
[44] Kricheldorf HR, Domschke A. Macromolecules 1996;29:1337–44.
[45] Michaels AS, Parker RB. J Polym Sci 1959;41:53–71.
[46] Michaels AS, Bixler HJ. J Polym Sci 1961;50:393–412.
[47] Puleo AC. PhD dissertation, The University of Texas at Austin (1988).
[48] Manfredi C, Nobile MAD, Mensitieri G, Guerra G, Rapacciuolo M. J Polym Sci, Part B: Polym Phys 1997;35:133–40.
[49] Guadagno L, Baldi P, Vittoria V, Guerra G. Macromol Chem Phys 1998;199:2671–5.
[50] Ly YP, Cheng Y. J Membr Sci 1997;133:1997.
[51] Mogri Z, Paul DR. J Membr Sci 2000;175:253–65.
[52] Koros WJ. PhD dissertation, The University of Texas at Austin (1977).
[53] Broadhurst MG. J Res Natl Bur Stand, Sect A 1962;66A:241–9.
[54] Lee JL, Pearce EM, Kwei TK. Macromolecules 1997;30:6877–83.
[55] Platé NA, Shibaev VP, Petrukhin BS, Kargin VA. J Polym Sci, Part C 1968;23:37–44.
[56] Alig I, Jarek M, Hellmann GP. Macromolecules 1998;31:2245–51.
[57] Chiou JS, Barlow JW, Paul DR. J Appl Polym Sci 1985;30:1173–86.
[58] Bixler HJ, Sweeting OJ. In: Sweeting OJ, editor. Barrier properties of films, The science and technology of polymer films, vol. 2. New York: Wiley, 1971.